Chemical Engineering Journal 358 (2019) 362–368

Contents lists available at ScienceDirect

Chemical Engineering Journal

journal homepage: www.elsevier.com/locate/cej

N-doped carbon-wrapped Mo_xC heterophase sheets for high-efficiency electrochemical hydrogen production

Tanli Xiong[a,1], Jin Jia[a,1], Zhaoqian Wei[a,1], Lili Zeng[a], Yunqie Deng[a], Weijia Zhou[a,*], Shaowei Chen[a,b,*]

[a] Guangzhou Key Laboratory for Surface Chemistry of Energy Materials, New Energy Research Institute, School of Environment and Energy, South China University of Technology, Guangzhou Higher Education Mega Center, Guangzhou, Guangdong 510006, PR China
[b] Department of Chemistry and Biochemistry, University of California, 1156 High Street, Santa Cruz, CA 95064, USA

HIGHLIGHTS

- N doped carbon-wrapped Mo_xC heterophase sheets are synthesized via in situ carbonation.
- N-Mo_xC@C HSs effectively combine the respective advantages of both γ-MoC and β-Mo_2C.
- Heterostructures possess a synergistically-enhanced activity on the interface and surface of γ-MoC/β-Mo_2C.
- N-Mo_xC@C HSs exhibit excellent activity and stability in acid media.

ARTICLE INFO

Keywords:
Molybdenum carbide
Heterophase
Mo sheets
Nitrogen doping
Carbon wrapping
Hydrogen evolution reaction

ABSTRACT

Advancement of non-precious-metal catalysts for hydrogen evolution reactions (HER) with both prominent activity and excellent stability has been becoming an ongoing challenge in the following decades. Herein, N-doped carbon-wrapped molybdenum carbide heterophase (γ-MoC and β-Mo_2C) sheets (N-Mo_xC@C HSs) were prepared by a facile chemical vapor reduction (CVR) procedure and following calcination at desired temperatures. The best HER electrocatalytic activity of N-Mo_xC@C HSs was detailedly examined in 0.5 M H_2SO_4, which exhibited a small overpotential of 172 mV (10 mA cm^{-2}) with a Tafel slope of only 60 mV dec^{-1} and durability. The improved HER activities and catalytic stability were due to heterocrystal Mo_xC, nitrogen doping, and carbon coating. Particularly, this study effectively combined the respective advantages of both γ-MoC and β-Mo_2C via the interface effect and matched polarity of hydrogen adsorption.

1. Introduction

Electrocatalytic hydrogen evolution is regarded to be an efficient way of producing high energy density, clean, and sustainable hydrogen that can be an alternative for next generation energy. The hydrogen evolution reactions (HER) of water electrolysis essentially depend on the efficiency of electrocatalysts, which should be durable and able to diminish overpotentials close to its thermodynamic value for water electrolysis. Several noble-metal catalysts, such as Pt-based materials, hold extraordinary efficiency and productivity in the HER of water splitting, nevertheless, their extreme scarcity and high price hinder their widely industrial applications [1]. Hence, worldwide attention has been attracted to contrive and explore non-noble-based catalysts [2–4]. Of late, molybdenum-based compounds, for example molybdenum disulfide (MoS_2), [5–8] molybdenum selenide ($MoSe_2$), [9,10] molybdenum diboride (MoB_2), [11,12] molybdenum carbide (Mo_2C and/or MoC), [13–16] molybdenum phosphide (MoP), [17–19] and molybdenum nitride (MoN), [20,21] have been gradually developed as electrocatalysts for water splitting in acidic condition. In the midst of these Mo-based materials, Mo_xC displays marvelous HER activities under both basic and acidic electrolytes owing to its analogous electronic structures to the d-orbital of Pt and its potential application as a low-cost, efficient HER electrocatalyst [22]. In this regard, molybdenum carbide (Mo_xC) with an electron configuration similar to that of Pt can act as a new promising platinum alternative catalyst for HER. Since the first investigation of Mo_xC microparticles in the application of

* Corresponding authors at: Guangzhou Key Laboratory for Surface Chemistry of Energy Materials, New Energy Research Institute, School of Environment and Energy, South China University of Technology, Guangzhou Higher Education Mega Center, Guangzhou, Guangdong 510006, PR China.
E-mail addresses: eszhouwj@scut.edu.cn (W. Zhou), shaowei@ucsc.edu (S. Chen).
[1] These authors contributed equally to the work.

https://doi.org/10.1016/j.cej.2018.09.047
Received 3 January 2018; Received in revised form 28 August 2018; Accepted 6 September 2018
Available online 07 September 2018
1385-8947/

electrocatalytic hydrogen evolution, there have been intensive efforts to fabricate various Mo_xC-based electrocatalysts because of the advantages of low cost, excellent conductivity, high catalytic activity, and stability. To improve the activity of bulk Mo_xC for HER, nano/microstructure design is often employed during the preparation of Mo_xC composites, ranging from zero-dimensional (0D) nanoparticles to one-dimensional (1D) rods/wires/tubes/fibers, even two-dimensional (2D) or three-dimensional (3D) complex structures [14,15,23–29]. The major purpose is to maximize the exposed active surface and optimize the phase/electronic structure of Mo_xC, and thus realize significant improvement of electrocatalytic activity towards HER. Apart from exploring various novel nano/microstructured Mo_xC, heteroatom doping has proved to be an effective strategy for enhancing HER kinetics. On the one hand, heteroatom doping could tune the d-orbitals of Mo_xC and modify the Fermi level, subsequently tuning the activity of Mo_xC. On the other hand, heteroatoms themselves and their adjacent atoms may also serve as additional active sites. Dopants are frequently non-metal atoms, for instance nitrogen, [30] phosphorus, [31] and sulfur [32]. Non-metal heteroatom doping involves the replacement of carbon atoms in Mo_xC crystals or carbon support material, and thus induces the modification of the electronic structure and surface chemistry of electrocatalysts.

Particularly, the valence band shapes of β-Mo_2C and γ-MoC are very similar to that of Pt, except β-Mo_2C has a slightly higher density around Fermi level than γ-MoC, which also makes β-Mo_2C less stable [33,34]. γ-MoC is theoretically the most stable stoichiometric (1:1) phase, however γ-MoC has the strongest antioxidant capacity followed by β-Mo_2C, α-MoC_{1-x}, and η-MoC, which matches the order of stability from previous theoretical and experimental studies [15,33,35]. A more Pt-like Fermi level energy in β-Mo_2C and γ-MoC is a possible and necessary condition for great HER catalytic activity. Recently, Brian M. Leonard et al. reported β-Mo_2C and γ-MoC respectively exhibited the first and second highest HER activity among all four phases of molybdenum carbide (α-MoC_{1-x}, β-Mo_2C, γ-MoC, and η-MoC) in acidic solution and considered the reason that γ-MoC showed lower activity for HER than β-Mo_2C is that γ-MoC had smaller surface area [15]. In a word, γ-MoC is the most stable phase among all four phases of molybdenum carbide basing on both theoretical and experimental results. Prof. Gao and Prof. Tang et al reported that as-synthesized η-MoC/α-Mo_2C heteronanowires composed of well-defined nanoparticles via restrained carbonization, indicating outstanding HER activities, rapid kinetic metrics and excellent stability in both acid and basic conditions [14]. Apart from the phase, composition, crystal and electronic structure, the morphology, size and carbon layer are another three possible factors that affect the catalytic activity for HER. Combining the respectively promoted elementary reactions of HER on β-Mo_2C (strong hydrogen adsorption and prominent activity) and γ-MoC (strong hydrogen desorption and excellent stability), it's promising to design a synergistically-enhanced activity on the interface and surface of γ-MoC/β-Mo_2C, however as far as we know, which is hardly ever reported.

Herein, we demonstrated a facile and novel strategy for synthesizing N-doped carbon-wrapped molybdenum carbide heterophase sheets (N-Mo_xC@C HSs) as efficient and stable HER electrocatalyst, which are composed of γ-MoC and β-Mo_2C phases with carbon wrapped and nitrogen doped and ameliorated activity by varying synthesis temperature. The carbon layers wrapped the electrocatalysts not only protected dissolution and surface oxidation in acidic condition, but also not affected the catalytic activity as a result of interfacial charge transfer [36–38]. With favorable abundant exposed surface-active sites, short diffusion distances, and multiple electron/electrolyte/gas separations and transfer pathways, this specially designed N-Mo_xC@C HSs greatly facilitate the hydrogen production and release, which exhibits a small overpotential of 172 mV to equal to 10 mA cm^{-2} and a small Tafel slope of only 60 mV dec^{-1}, accompanied by an extremely large cathodic current density and superior stability in 0.5 M H_2SO_4 solution.

2. Experiment section

2.1. Materials

All reagents were of analytical grade and used without further purification. Molybdenum trioxide (MoO_3), dicyandiamide (DCDA, $C_2H_4N_4$), sulfuric acid (H_2SO_4), and 20 wt% Pt/C were purchased from Alfa Aesar. Nafion solution (10% Nafion in ethanol) was purchased from Sigma-Aldrich. Argon and hydrogen gas mixture (Ar-H_2, 10% H_2) was purchased from Guangzhou YIGAS Gases CO., LTD.

2.2. Synthesis of N-Mo_xC@C HSs

Mo sheets (Mo Ss) were synthesized on quartz tube wall in a quartz tube furnace by combining the sublimation of MoO_3 and reduction by Ar-H_2 mixture gas at 900 °C.[19] The obtained Mo sheets and DCDA were placed into a covered crucible in a tube furnace (The dimension of the quartz tube is Φ50 mm*L600 mm.) by simple normal mixing, which were heated at 450 °C for 2 h, then heated up to the controlled temperatures (750 °C, 850 °C, 950 °C, or 1050 °C) for 2 h under a Ar atmosphere (~10 sccm) with a heating speed of 5 °C min^{-1}, respectively, to produce the different N-doped and carbon-wrapped molybdenum carbide heterophase sheets (N-Mo_xC@C HSs-T, T stands for the synthesis temperature). Finally, black N-Mo_xC@C HSs-T electrocatalysts were obtained when the furnace cooled down naturally to room temperature.

3. Results and discussion

The overall strategy for the synthesis of N-modified and C-wrapped molybdenum carbide heterosheets (denoted as N-Mo_xC@C HSs) was schematically presented in Scheme 1, and the detailed procedure was described in the experimental section. To prepare the N-Mo_xC@C HSs, we first produced the Mo Ss via chemical vapor reduction (CVR) between sublimation of MoO_3 and reduction of H_2 according to our previously reported method [19]. From Fig. S1, the MoO_3 starting materials were just ordinary powder particles. Field Emission Scanning electron microscope (FESEM) was implemented to examine the morphologies and structures of as-synthesized Mo Ss as shown in Figs. 1a, b and S2a, b, which possessed the size of a few microns and thickness of ~50 nm. The Mo Ss possessed the dendritic slices due to the metastable state of Mo during equilibrium between sublimation of MoO_3 and reduction of Ar-H_2 at high temperature. Subsequently, the as-prepared Mo Ss were directly annealed with DCDA at 950 °C in Ar gas flow to produce dark grey Mo_xC HSs encapsulated by the carbon shell and modified by nitrogen atoms. The obtained N-Mo_xC@C HSs-950 possessed the convex-concave surface (Figs. 1c, d and S2c, d), and similar size and enlarged thickness (~80 nm). After the followed

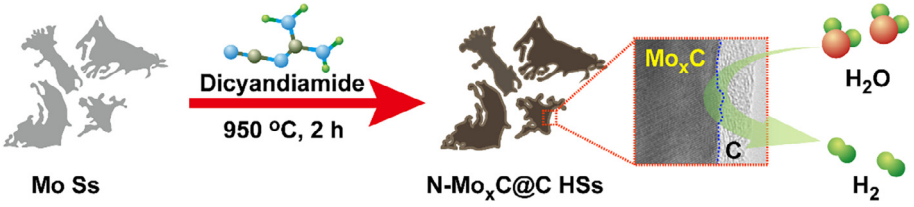

Scheme 1. Schematic illustration for the preparation of N-Mo_xC@C HSs from Mo Ss with dicyandiamide at tunable temperature.

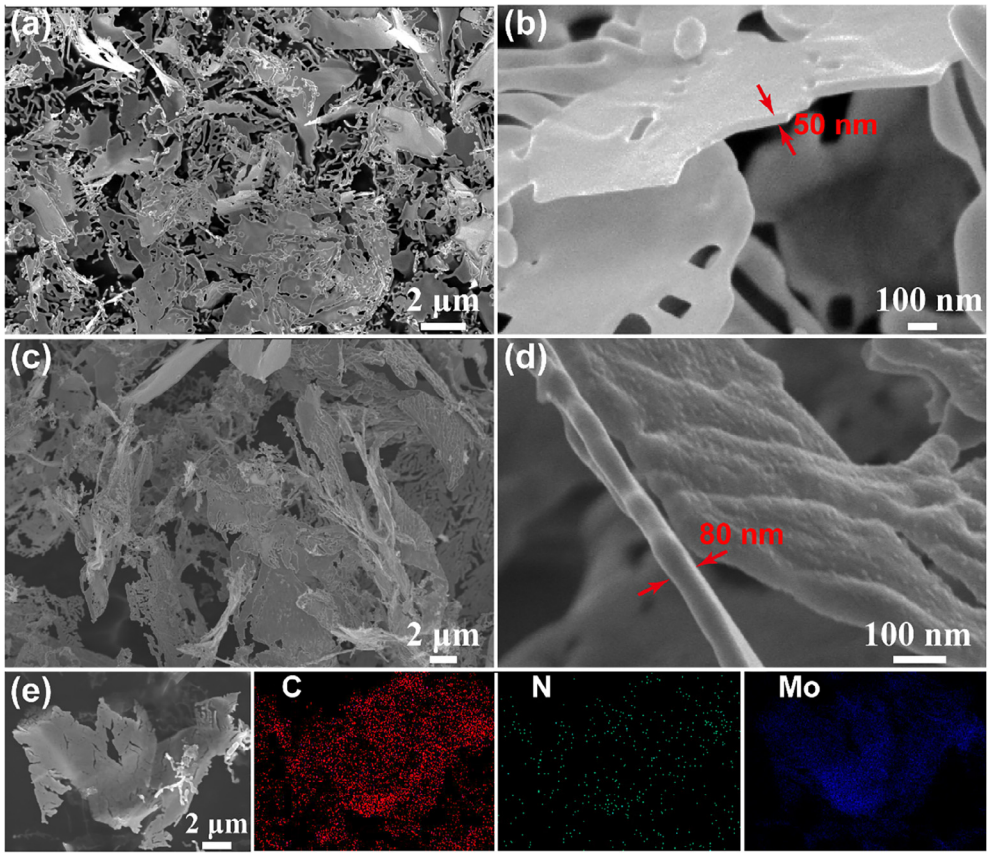

Fig. 1. SEM of (a, b) Mo Ss and (c, d) N-Mo_xC@C HSs-950. (e) The C/N/Mo mapping of N-Mo_xC@C HSs-950.

calcining process with dicyandiamide at high temperature, the sheets morphology of as-obtained N-Mo_xC@C HSs-950 was inherited, which did not reveal apparent variation whereas demonstrated good thermostability of N-Mo_xC@C HSs-950. Besides, energy-dispersive X-ray spectrometry (EDS) element mapping of a large fluffy area (Fig. 1e) exhibits well spatial distribution of C, N and Mo elements throughout the observed area, implying a successful and uniform distribution of target material, N-Mo_xC@C HSs-950. In addition, the SEM images of N-Mo_xC@C HSs synthesized at 750 °C, 850 °C, and 1050 °C were shown in Fig. S3, which confirmed the sheet morphologies were remained at the high calcination temperatures.

These phase changes during the synthesis steps were firstly studied by XRD patterns of samples at different reaction temperatures as shown in Fig. 2a. The synthesized Mo sheets showed the characteristic diffraction peaks at 40.5° (1 1 0), 58.6° (2 0 0), 73.6° (2 1 1), and 87.6° (2 2 0) (Cubic, Im3 m (2 2 9), PDF no. 42-120). Similar XRD patterns assigned to main hexagonal γ-MoC (WC type, P6m2, PDF no. 45-1015) and a small quantity of hexagonal β-Mo_2C (Fe_2N type, P63/mmc, PDF no. 35-0787) were clearly observed between 750 °C and 1050 °C. The characteristic diffraction peaks at 32° (0 0 1), 36° (1 0 0), 48.7° (1 0 1), 64.5° (1 1 0), 66.4° (0 0 2), 73.8° (1 1 1), 76° (2 0 0), 78° (1 0 2), and 85° (2 0 1) for γ-MoC and 34.6° (1 0 0), 37.8° (0 0 2), 39.6° (1 0 1), 52.2° (1 0 2), 61.8° (1 1 0), 69.4° (1 0 3), 72.5° (2 0 0), 75° (1 1 2), and 85° (2 0 2) for β-Mo_2C were observed, respectively. The corresponding crystal structures of γ-MoC and β-Mo_2C were shown in Figs. S4 and S5. It was clear that the temperature had a negligible impact on the formation of the crystal phases between 750 °C and 1050 °C. No extra peaks corresponding to metallic Mo and MoO_x were observed.

Noticeably, in comparison with N-Mo_xC@C obtained at 750 °C and 1050 °C, the (1 0 0) and (1 0 1) diffraction peaks at 2θ ~ 36° and 2θ ~ 39.6° of γ-MoC and β-Mo_2C in N-Mo_xC@C HSs obtained at 850 °C and 950 °C showed a slight shift of ~0.2° to higher diffraction angle (Fig. 2b). It was noteworthy that diffraction peak of (0 0 1) in β-Mo_2C was located at the same angle, implying that the shift of the (1 0 0) and (1 0 1) diffraction peaks were not due to the testing error. The possible reason was that the N doping caused the lattice distortion, which was confirmed by changed N doping amount with calcination temperature (Fig. 2c). Namely, the shift of the (1 0 0) and (1 0 1) diffraction peaks were possibly due to doping N into the lattice, which caused the decrease of the lattice parameters of *a*/*b* in γ-MoC and β-Mo_2C (Fig. 2b). Moreover, the resulting carbon shells were also doped with some nitrogen atoms (Fig. S6), which mainly survived in the form of pyridinic N atoms (Fig. 2c). This phenomenon was congruent with the N, Fe, Co or Ni-doped Mo_2C, [24,25,32,39] and the substitutions of certain C atoms with smaller N atoms in lattice led to the shrink of Mo_xC unit cell.

XPS measurements were executed to thoroughly analyse the elemental composition and valence of the Mo Ss and N-Mo_xC@C HSs samples. The XPS spectra of N 1s showed that N doping amounts of samples obtained at different temperatures were different in Fig. 2c. The N 1s XPS spectrum showed two N peaks at 398.2 and 401.1 eV, which respectively originated from the pyridinic N and graphitic N. Due to their lone-pair electrons, these species of N can synergistically tune the electron density on the surface of carbon layers with the wrapped Mo_xC HSs. Compared to N doping amount of 17.45 at% in N-Mo_xC@C HSs-850, the decreased value (14.7 at%) of N-Mo_xC@C HSs-750 was due to the inadequate doping at low calcination temperature. Also, the decreased N doping amounts of N-Mo_xC@C HSs-950 (7.92 at%) and Mo_xC@C HSs-1050 (~1 at%) were attributed to the decomposition of unstable N doping structure at high calcination temperature. In addition, XPS spectra of the detected Mo 3d core level showed that the main Mo^{3+} with peaks at 228.7 eV and 231.9 eV (Mo 3d5/2 and Mo 3d3/2) and Mo^{2+} with peaks at 228.2 eV and 231.3 eV (Mo 3d5/2 and Mo 3d3/2) were observed in N-Mo_xC@C HSs (Fig. 2d). The Mo^{4+} species from MoO_2 at 232.9 eV (Mo 3d3/2) and 230 eV (Mo 3d5/2) and Mo^{6+}

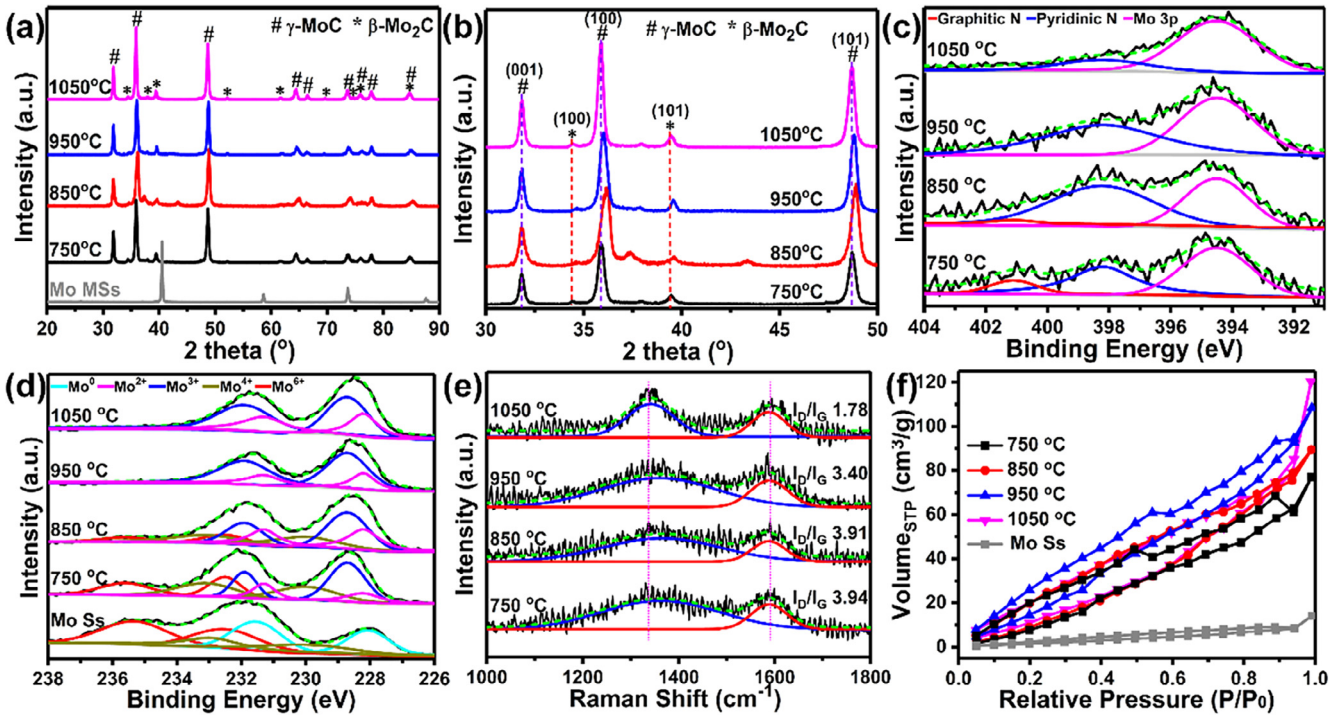

Fig. 2. (a, b) XRD patterns, XPS spectrum of (c) N 1s and (d) Mo 3d (e) Raman spectra, and (f) N_2 adsorption-desorption isotherms of the samples obtained at different temperature.

species from MoO_3 at 235.8 eV (Mo 3d3/2) and 232.5 eV (Mo 3d5/2) were also detected in Mo Ss, N-Mo_xC@C HSs-750 °C, and N-Mo_xC@C HSs-850 °C due to an oxidic surrounding of exposed air, both of which were thought to be inactive for HER. Mo^{3+} and Mo^{2+} are designated as γ-MoC and β-Mo_2C respectively, thus implying heterophases of the Mo_xC HSs. The Mo^{2+} and Mo^{3+} species are intensively studied, since which are the active sites and centres for electrocatalytic reaction of HER. The Mo^{3+}/Mo^{2+} mole ratios ($m_{3+/2+}$) on the Mo_xC surface are capable of providing valuable information to recognize the nature of the active sites, due to the dominance of Mo^{2+} in Mo_2C and the ascendency of Mo^{3+} in MoC (Table S1). In the heterostructures, $m_{3+/2+}$ visibly changed between 1.4 and 2.9 for N-Mo_xC@C HSs at different temperature. Such a variation of $m_{3+/2+}$ will influence the HER activity, correlated with the different electron density around Mo^{3+} and Mo^{2+}. However, no oxidized state of Mo was observed in N-Mo_xC@C HSs-950/1050, implying the carbon coating protected the surface of molybdenum carbide from oxidation.

Raman spectra of N-Mo_xC@C HSs (Fig. 2e) exhibited two characteristic peaks located at ~1355 cm^{-1} and 1595 cm^{-1}, ascribed to the well-documented D and G bands of carbon shell separately, and confirmed the presence of carbon in N-Mo_xC@C HSs. The carbon coating can protect the surface of molybdenum carbide from oxidation, which was confirmed by XPS. In addition, the carbon coating also constructed a hierarchically porous structure and increased the specific surface area, which was confirmed by N_2 adsorption-desorption isotherms as shown in Fig. 2f and Table S2. Compared to the specific surface area of Mo sheets (~6 $m^2 g^{-1}$), the specific surface area of N-Mo_xC@C HSs were 16–21 times larger for N-Mo_xC@C HSs-750 (99.9 $m^2 g^{-1}$), N-Mo_xC@C HSs-850 (103.2 $m^2 g^{-1}$), N-Mo_xC@C HSs-950 (109.6 $m^2 g^{-1}$) and N-Mo_xC@C HSs-1050 (102.5 $m^2 g^{-1}$). In addition, the primary pore size distributions at 1–8 nm and average pore diameter ~2 nm were observed for these N-Mo_xC@C HSs (Fig. S7). This sufficiently confirmed that some micro/mesopores existed in these materials, which were favorable for mass transport and adsorption. As a general rule, the relatively increased exposing surface of the Mo_xC hybrids would contribute their electrocatalytic performances and properties positively in addition to the intensive contribution from electronic modulation between γ-MoC and β-Mo_2C within the Mo_xC hybrids, as minutely studied in the above-mentioned XPS sections.

TEM measurements were performed to further characterize the morphology and crystal structure of N-Mo_xC@C HSs-950. As shown in Fig. 3a, Mo Ss were mainly lamellar and dendritic slices. Note that only the long-range crystalline lattices of 0.22 nm were observed in Mo Ss (Fig. 3b), corresponding to (1 1 0) of body-centered cubic (bcc) Mo. Some noticeable oxide coating on the edge of Mo Ss can be observed and not detected by XRD because of the low content, but was confirmed by the corresponding XPS result (Fig. 2d). After carbonization, the coarse N-Mo_xC@C HSs-950 sheets possessed the crystalline lattices of 0.19 nm and 0.23 nm corresponded to the (1 0 1), (1 0 1) plane of γ-MoC and β-Mo_2C, separately (Fig. 3d and Figs. S8–10). In addition, the carbon coating with thickness of ~3 nm on surface of γ-MoC was observed and the according crystalline lattices of 0.32 nm were detected (Fig. 3d, e), and the carbon layer belong to graphitic carbon (Fig. S6). EDS element mapping of a selected N-Mo_xC@C HSs-950 showed that the C, N and Mo elements were indeed uniformly dispersed in the sheet, implying the successful synthesis of N doped Mo_xC sheets (Fig. 3e–h).

To investigate the HER performance of Mo Ss and N-Mo_xC@C HSs in an acidic electrolyte, Fig. 4a displayed their polarization curves in 0.5 M H_2SO_4, accompanied by that of the 20 wt% Pt/C catalysts for reference. Among the N-Mo_xC HSs samples, N-Mo_xC@C HSs-950 exhibited the optimum electroactivity for HER. To achieve 10 mA cm^{-2}, N-Mo_xC@C HSs-950 required a η_{10} of 172 mV, obviously better than those of Mo Ss (320 mV), N-Mo_xC@C HSs-750 (275 mV), N-Mo_xC@C HSs-850 (218 mV) and N-Mo_xC@C HSs-1050 (303 mV). Such a synergic N doping effect was prohibited at the high synthesis temperature of 1050 °C, and the HER activity obviously reduced due to the decreased nitrogen doping amount.

Correspondingly, the Tafel plots showed the same trend in HER kinetics (Fig. 4b). Among them, N-Mo_xC@C HSs-950 showed a Tafel slope of 60 mV dec^{-1}, which was apparently preferable than those of Mo Ss (94 mV dec^{-1}), N-Mo_xC@C HSs-750 (80 mV dec^{-1}), N-Mo_xC@C HSs-850 (69 mV dec^{-1}) and Mo_xC@C HSs-1050 (85 mV dec^{-1}). The

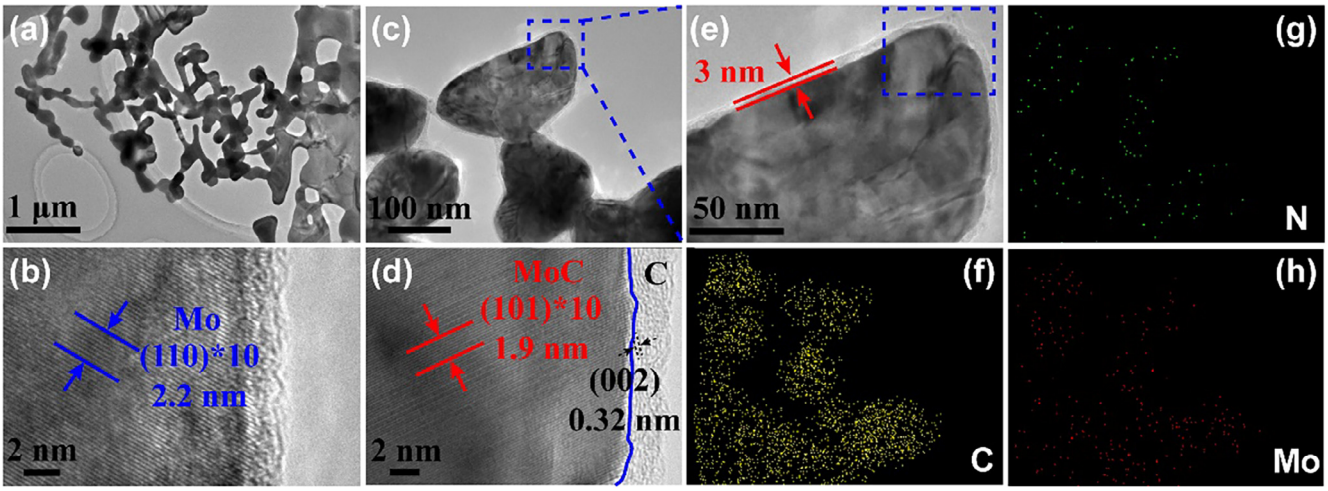

Fig. 3. (HR) TEM images of (a, b) Mo Ss, and (c, d) N-Mo$_x$C@C HSs-950; (e) higher amplification of the blue box in (c); (g–h) EDX mapping of the N-Mo$_x$C@C HSs-950. (For interpretation of the references to colour in this figure legend, the reader is referred to the web version of this article.)

suitable Tafel slope of N-Mo$_x$C@C HSs indicated a speedy enhancement of the hydrogen production rate with the operated overpotential, corresponding to the great activity shown in the polarization curve. As reported by the classic theory, the HER of electrolyze water in acidic aqueous electrolyte process involved in three steps: $H^+ + e^- \rightarrow H^*$ (Volmer reaction), $H^+ + e^- + H^* \rightarrow H_2$ (Heyrovsky reaction), and $H^* + H^* \rightarrow 2^* + H_2$ (Tafel reaction). The first one was an electrochemical reduction step (H^+ reduction) with Tafel slope of ~120 mV dec^{-1}, and the second one (H_{ads} desorption) was either the ion and atom reaction with Tafel slope of ~40 mV dec^{-1} or the atom combination reaction with Tafel slope of ~30 mV dec^{-1}. Although the only Tafel slope was inadequate to identify the specific mechanism, the demonstrably reduced slope for N-Mo$_x$C@C HSs-950, compared with Mo Ss, N-Mo$_x$C@C HSs-750, N-Mo$_x$C@C HSs-850, and N-Mo$_x$C@C HSs-1050, still confirmed the improved Volmer step in the HER kinetics of water splitting. Additionally, the exchange current density (j_0) of the aforesaid catalysts was also reckoned by extrapolating Tafel plots, which was the intrinsic mensuration of HER activity. As is expected, the j_0 of 0.03 mA cm^{-2} for N-Mo$_x$C@C HSs-950 was higher than that of the other N-Mo$_x$C@C HSs (Fig. S11).

Fig. 4c exhibited the typical Nyquist plots of the N-Mo$_x$C@C HSs and Mo Ss-modified glassy-carbon electrodes collected at an HER overpotential of 200 mV. Further detailed analyses were implemented by fitting the impedance spectra to an equivalent circuit with the CPE (inset of Fig. 4c). The R_{ct} of the N-Mo$_x$C@C HSs-950 electrode (27 Ω) was found to be obviously smaller than these of the Mo Ss (~120 Ω), N-

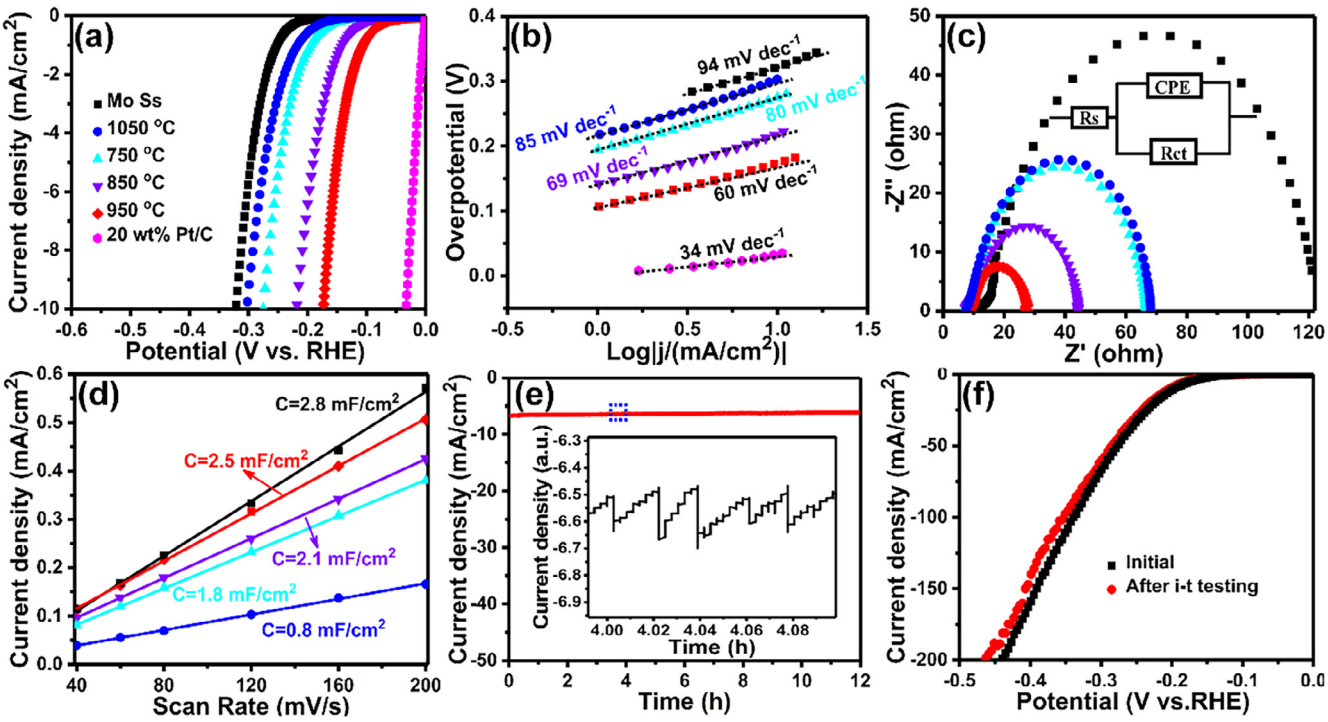

Fig. 4. (a) HER polarization curves and (b) Tafel plots of Mo Ss, N-Mo$_x$C@C HSs-750, N-Mo$_x$C@C HSs-850, N-Mo$_x$C@C HSs-950, Mo$_x$C@C HSs-1050 and 20 wt% Pt/C, respectively. (c) Nyquist plots and (d) Capacitive currents as a function of scan rates with various rates from 40 to 200 mV s^{-1} of Mo Ss, N-Mo$_x$C@C HSs-750, N-Mo$_x$C@C HSs-850, N-Mo$_x$C@C HSs-950 and Mo$_x$C@C HSs-1050, respectively. (e) Long-term durability test of N-Mo$_x$C@C HSs-950 at −165 mV for 12 h. Inset is enlargement of the area denoted by the blue dashed circle. (f) Polarization curves of N-Mo$_x$C@C HSs-950 before and after i-t testing.

Mo_xC@C HSs-1050 (68 Ω), N-Mo_xC@C HSs-750 (66 Ω) and N-Mo_xC@C HSs-850 (44 Ω), indicating that the greatly conductive Mo_xC@C substrates lessened the resistance of the heterophase electrocatalysts of N-Mo_xC@C HSs-950. In addition, from Fig. S12, it can be seen that R_{ct} of N-Mo_xC@C HSs-950 reduced considerably with progressive overpotentials, from 112 Ω at 200 mV to 27 Ω at 300 mV, as proved by the evident reduction of the diameter of the semicircles.

The strong correlation between the HER catalysis and electrochemical area of Mo Ss and N-Mo_xC@C HSs was accessed by electrochemical double layer capacitance (Fig. 4d). The capacitance of N-Mo_xC@C HSs-950 was 2.5 mF cm^{-2}, larger than those of N-Mo_xC@C HSs-750 (1.8 mF cm^{-2}), N-Mo_xC@C HSs-850 (2.1 mF cm^{-2}) and N-Mo_xC@C HSs-1050 (0.8 mF cm^{-2}). However, after being corrected by electrochemical area, the HER performance of N-Mo_xC@C HSs-950 still possessed the lowest onset potential (Fig. S13), implying that the larger electrochemical area only increased the number of active sites, but was not the nature for enhanced HER activity. The number of active sites was also inferred from the electrochemically active surface area (ECSA), and we calculated ECSA by the specific capacitance (see the Supporting information for details on the calculation). It was worth noting that the CV curves of the N-Mo_xC@C HSs-950 had a nearly rectangular shape (Fig. S14), indicating the high electrical conductivity.

Aside from wonderful catalytic activity, the N-Mo_xC@C HSs-950 also exhibited excellent stability for HER. To further investigate the stability of N-Mo_xC@C HSs-950 in HER, the long-term durability test of N-Mo_xC@C HSs-950 at −165 mV for 12 h were collected in Fig. 4e. The reduction current density continued approximate attenuation over 12 h of unceasing working, demonstrating exceptional durability of N-Mo_xC@C HSs-950 for HER in 0.5 M H_2SO_4. The as-gauged i-t curve was in a characteristic serrate profile, which follows from the alternative processes of bubble cumulation and bubble release. To compare data, the variation of current density frequently fluctuates less than 0.15 mA cm^{-2} before and after bubble release, signifying that the bubbles are able to readily release on the surface of N-Mo_xC@C HSs-950. Fig. 4f showed that, after i-t testing, the polarization curves of the N-Mo_xC@C HSs-950 electrode remained almost unchanged. Because the negative hydrogen binding energy on Mo_2C indicates a strong adsorption of H ions on the surface of β-Mo_2C, that facilitates H^+ reduction (Volmer step), however hinders H_{ads} desorption (Heyrovsky step or Tafel step). Yet, γ-MoC works in reverse [40]. So, this efficient bubble release and effective electron regulation are probably originated from the heterophase construction of N-Mo_xC@C HSs-950. Fig. S15 confirmed that the N-Mo_xC@C HSs-950 possessed good structural stability as well as catalytic stability after i-t testing.

All these results indicated that N-Mo_xC@C HSs was an excellent active material for Mo-based HER catalysts and displayed excellent electrochemical properties. Mechanism of N-Mo_xC@C HSs for high efficiency electrochemical hydrogen production should be attributed to two aspects. Firstly, the highly catalytic activities of catalysts are originated from the controllable structure, which requires a specific synthesis method to prepare it. Secondly, a quadplex synergistic effect has been achieved for the HER. 1) The first synergistic effect from homogeneously dispersed γ-MoC and β-Mo_2C phases can improve the intrinsic activity and conductivity of Mo_xC. 2) The second synergistic effect from homogeneously N-doped Mo_xC phases can improve the intrinsic activity and conductivity of Mo_xC. 3) The third synergistic effect from the Mo_xC and N-doped C shell can enhance the density of active sites and conductivity of Mo_xC. 4) The forth synergistic effect from N-doped C can accelerate the charge transfer rate and improve close interaction between NC and Mo_xC. Additionally, the high electrochemical area due to porous sheet structure and carbon coating got access to highly exposed reactive sites. In brief, the modifications of the Mo_xC hybrid, nitrogen doping, and carbon coating in structure and surface area would play a significant role in the improvement of the electrocatalytic HER property.

Strikingly, the N-Mo_xC@C HSs possessed the integrated HER performance with onset potential of −106 mV, Tafel value of 60 mV dec^{-1} and low overpotential (172 mV at 10 mA cm^{-2}), which performed superior or close to majority of the documented non-precious-metal electrocatalysts in acidic electrolytes, such as Mo_2C/GCSs (onset potential of −120 mV, Tafel value of 62.6 mV dec^{-1}, and overpotential of 200 mV at 10 mA cm^{-2}), [41] Mo_2C nanowires (onset potential of −70 mV, Tafel value of ~53 mV dec^{-1}, and overpotential of ~200 mV at 10 mA cm^{-2}), [26] Mo_2C/CNT-graphene (onset potential of −62 mV, Tafel value of 62 mV dec^{-1}, and low overpotential of 172 mV at 10 mA cm^{-2}), [42] Mo_2C (onset potential of −105 mV, Tafel value of 70 mV dec^{-1}, and overpotential of 192 mV at 10 mA cm^{-2}), [29] Mo_2C-C (onset potential of −100 mV, Tafel value of 85 mV dec^{-1}, and overpotential of 164 mV at 10 mA cm^{-2}),[43] which were listed in the Supporting information (Table S3).

4. Conclusions

To sum up, a new powerful strategy to remarkably boost the electrocatalytic activity of N-Mo_xC@C HSs-950 by introducing molybdenum sheets as template has been demonstrated. By means of thermal treatment with C and N atmosphere pyrolyzed from dicyandiamide, Mo_xC heterophase with γ-MoC and β-Mo_2C and N dopants are successfully induced into N-Mo_xC@C HSs, enabling the resulting abundant active sites. The N-Mo_xC@C HSs-950 showed outstanding HER performance, with a proper overpotential of 172 mV and an appropriate Tafel slope of 60 mV dec^{-1}. Moreover, this N-Mo_xC@C HSs-950 electrode yields an excellent long-term durability. Our results demonstrate that the constructing complementary heterogeneity of γ-MoC/β-Mo_2C are a potential candidate to the expensive and scarce Pt for low-cost electrocatalyst. Our findings here may deepen the understanding of the role of heterophase, furthermore nitrogen doping and carbon wrapping may provide new insights into developing high-performance electrocatalyst for water splitting.

Acknowledgements

This work was supported by Tip-top Scientific and Technical Innovative Youth Talents of Guangdong Special Support Program (2016TQ03N541), Guangdong Natural Science Funds for Distinguished Young Scholar(2017B030306001), the National Natural Science Foundation of China (51502096, 91745203) and Guangdong Innovative and Entrepreneurial Research Team Program (2014ZT05N200).

Appendix A. Supplementary data

Supplementary data associated with this article can be found, in the online version, at https://doi.org/10.1016/j.cej.2018.09.047.

References

[1] N. Cheng, S. Stambula, D. Wang, M.N. Banis, J. Liu, A. Riese, B. Xiao, R. Li, T.-K. Sham, L.-M. Liu, Platinum single-atom and cluster catalysis of the hydrogen evolution reaction, Nat. Commun. 7 (2016) 13638.
[2] W.J. Zhou, J. Jia, J. Lu, L.J. Yang, D.M. Hou, G.Q. Li, S.W. Chen, Recent developments of carbon-based electrocatalysts for hydrogen evolution reaction, Nano Energy 28 (2016) 29–43.
[3] J. Wang, F. Xu, H. Jin, Y. Chen, Y. Wang, Non-noble metal-based carbon composites in hydrogen evolution reaction: fundamentals to applications, Adv. Mater. 29 (2017) 1605838.
[4] M. Zeng, Y. Li, Recent advances in heterogeneous electrocatalysts for the hydrogen evolution reaction, J. Mater. Chem. A 3 (2015) 14942–14962.
[5] J. Xie, J. Zhang, S. Li, F. Grote, X. Zhang, H. Zhang, R. Wang, Y. Lei, B. Pan, Y. Xie, Correction to controllable disorder engineering in oxygen-incorporated MoS_2 ultrathin nanosheets for efficient hydrogen evolution, J. Am. Chem. Soc. 136 (2014) 1680–1680.
[6] Y. Wang, B. Chen, D.H. Seo, Z.J. Han, J.I. Wong, K. Ostrikov, H. Zhang, H.Y. Yang, MoS_2-coated vertical graphene nanosheet for high-performance rechargeable lithium-ion batteries and hydrogen production, NPG Asia Mater. 8 (2016) e268.
[7] J. Ding, Y. Zhou, Y. Li, S. Guo, X. Huang, MoS_2 nanosheet assembling superstructure

with a three-dimensional ion accessible site: a new class of bifunctional materials for batteries and electrocatalysis, Chem. Mater. 28 (2016) 2074–2080.
[8] L. Yang, W. Zhou, J. Lu, D. Hou, Y. Ke, G. Li, Z. Tang, X. Kang, S. Chen, Hierarchical spheres constructed by defect-rich MoS_2/carbon nanosheets for efficient electrocatalytic hydrogen evolution, Nano Energy 22 (2016) 490–498.
[9] S.J. Deng, Y. Zhong, Y.X. Zeng, Y.D. Wang, Z.J. Yao, F. Yang, S.W. Lin, X.L. Wang, X.H. Lu, X.H. Xia, J.P. Tu, Directional construction of vertical nitrogen-doped 1T–2H $MoSe_2$/graphene shell/core nanoflake arrays for efficient hydrogen evolution reaction, Adv. Mater. 29 (2017) 1700748.
[10] Y. Zhang, Q. Gong, L. Li, H. Yang, Y. Li, Q. Wang, $MoSe_2$ porous microspheres comprising monolayer flakes with high electrocatalytic activity, Nano Res. 8 (2015) 1108–1115.
[11] Y. Chen, G. Yu, W. Chen, Y. Liu, G.-D. Li, P. Zhu, Q. Tao, Q. Li, J. Liu, X. Shen, H. Li, X. Huang, D. Wang, T. Asefa, X. Zou, Highly active, nonprecious electrocatalyst comprising borophene subunits for the hydrogen evolution reaction, J. Am. Chem. Soc. 139 (2017) 12370–12373.
[12] H. Park, A. Encinas, J.P. Scheifers, Y. Zhang, B. Fokwa, Boron-dependency of molybdenum boride electrocatalysts for the hydrogen evolution reaction, Angew. Chem. Int. Ed. 129 (2017) 5667–5670.
[13] Y. Liu, G. Yu, G.D. Li, Y. Sun, T. Asefa, W. Chen, X. Zou, Coupling Mo_2C with nitrogen-rich nanocarbon leads to efficient hydrogen-evolution electrocatalytic sites, Angew. Chem. Int. Ed. 54 (2015) 10752–10757.
[14] H. Lin, Z. Shi, S. He, X. Yu, S. Wang, Q. Gao, Y. Tang, Heteronanowires of MoC-Mo_2C as efficient electrocatalysts for hydrogen evolution reaction, Chem. Sci. 7 (2016) 3399–3405.
[15] C. Wan, Y.N. Regmi, B.M. Leonard, Multiple phases of molybdenum carbide as electrocatalysts for the hydrogen evolution reaction, Angew. Chem. Int. Ed. 126 (2014) 6525–6528.
[16] J. Jia, W. Zhou, Z. Wei, T. Xiong, G. Li, L. Zhao, X. Zhang, H. Liu, J. Zhou, S. Chen, Molybdenum carbide on hierarchical porous carbon synthesized from Cu-MoO_2 as efficient electrocatalysts for electrochemical hydrogen generation, Nano Energy 41 (2017) 749–757.
[17] P. Xiao, M.A. Sk, L. Thia, X. Ge, R.J. Lim, J.-Y. Wang, K.H. Lim, X. Wang, Molybdenum phosphide as an efficient electrocatalyst for the hydrogen evolution reaction, Energy Environ. Sci. 7 (2014) 2624–2629.
[18] J. Yang, F. Zhang, X. Wang, D. He, G. Wu, Q. Yang, X. Hong, Y. Wu, Y. Li, Porous molybdenum phosphide nano-octahedrons derived from confined phosphorization in UIO-66 for efficient hydrogen evolution, Angew. Chem. Int. Ed. 128 (2016) 13046–13050.
[19] J. Jia, W. Zhou, G. Li, L. Yang, Z. Wei, L. Cao, Y. Wu, K. Zhou, S. Chen, Regulated synthesis of Mo sheets and their derivative MoX sheets (X: P, S, or C) as efficient electrocatalysts for hydrogen evolution reactions, ACS Appl. Mater. Interfaces 9 (2017) 8041–8046.
[20] J. Xie, S. Li, X. Zhang, J. Zhang, R. Wang, H. Zhang, B. Pan, Y. Xie, Atomically-thin molybdenum nitride nanosheets with exposed active surface sites for efficient hydrogen evolution, Chem. Sci. 5 (2014) 4615–4620.
[21] Y. Zhu, G. Chen, X. Xu, G. Yang, M. Liu, Z. Shao, Enhancing electrocatalytic activity for hydrogen evolution by strongly coupled molybdenum nitride@nitrogen-doped carbon porous nano-octahedrons, ACS Catal. 7 (2017) 3540–3547.
[22] M. Miao, J. Pan, T. He, Y. Yan, B.Y. Xia, X. Wang, Molybdenum carbide-based electrocatalysts for hydrogen evolution reaction, Chem. Eur. J. 23 (2017) 10947–10961.
[23] C.B. Lu, D. Tranca, J. Zhang, F.R. Hernandez, Y.Z. Su, X.D. Zhuang, F. Zhang, G. Seifert, X.L. Feng, Molybdenum carbide-embedded nitrogen-doped porous carbon nanosheets as electrocatalysts for water splitting in alkaline media, ACS Nano 11 (2017) 3933–3942.
[24] H. Lin, N. Liu, Z. Shi, Y. Guo, Y. Tang, Q. Gao, Cobalt-doping in molybdenum-carbide nanowires toward efficient electrocatalytic hydrogen evolution, Adv. Funct. Mater. 26 (2016) 5590–5598.
[25] S. Wang, J. Wang, M. Zhu, X. Bao, B. Xiao, D. Su, H. Li, Y. Wang, Molybdenum-carbide-modified nitrogen-doped carbon vesicle encapsulating nickel nanoparticles: a highly efficient, low-cost catalyst for hydrogen evolution reaction, J. Am. Chem. Soc. 137 (2015) 15753–15759.
[26] L. Liao, S. Wang, J. Xiao, X. Bian, Y. Zhang, M.D. Scanlon, X. Hu, Y. Tang, B. Liu, H.H. Girault, A nanoporous molybdenum carbide nanowire as an electrocatalyst for hydrogen evolution reaction, Energy Environ. Sci. 7 (2014) 387–392.
[27] W.F. Chen, C.H. Wang, K. Sasaki, N. Marinkovic, W. Xu, J.T. Muckerman, Y. Zhu, R.R. Adzic, Highly active and durable nanostructured molybdenum carbide electrocatalysts for hydrogen production, Energy Environ. Sci. 6 (2013) 943–951.
[28] H. Vrubel, X. Hu, Molybdenum boride and carbide catalyze hydrogen evolution in both acidic and basic solutions, Angew. Chem. Int. Ed. 51 (2012) 12703–12706.
[29] Z.Y. Wu, B.C. Hu, P. Wu, H.W. Liang, Z.L. Yu, Y. Lin, Y.R. Zheng, Z.Y. Li, S.H. Yu, Mo_2C nanoparticles embedded within bacterial cellulose-derived 3D N-doped carbon nanofiber networks for efficient hydrogen evolution, NPG Asia Mater. 8 (2016) e288.
[30] Y.Y. Chen, Y. Zhang, W.J. Jiang, X. Zhang, Z.H. Dai, L.J. Wan, J.S. Hu, Pomegranate-like N, P-doped Mo_2C@C nanospheres as highly active electrocatalysts for alkaline hydrogen evolution, ACS Nano 10 (2016) 8851–8860.
[31] Z.P. Shi, K.Q. Nie, Z.J. Shao, B.X. Gao, H.L. Lin, H.B. Zhang, B.L. Liu, Y.X. Wang, Y.H. Zhang, X.H. Sun, X.M. Cao, P. Hu, Q.S. Gao, Y. Tang, Phosphorus-Mo_2C@carbon nanowires toward efficient electrochemical hydrogen evolution: composition, structural and electronic regulation, Energy Environ. Sci. 10 (2017) 1262–1271.
[32] J. Jia, T.L. Xiong, L.L. Zhao, F.L. Wang, H. Liu, R.Z. Hu, J. Zhou, W.J. Zhou, S.W. Chen, Ultrathin N-doped Mo_2C nanosheets with exposed active sites as efficient electrocatalyst for hydrogen evolution reactions, ACS Nano 11 (2017) 12509–12518.
[33] H.W. Hugosson, O. Eriksson, L. Nordström, U. Jansson, L. Fast, A. Delin, J.M. Wills, B. Johansson, Theory of phase stabilities and bonding mechanisms in stoichiometric and substoichiometric molybdenum carbide, J. Appl. Phys. 86 (1999) 3758–3767.
[34] H.W. Hugosson, O. Eriksson, U. Jansson, B. Johansson, Phase stabilities and homogeneity ranges in 4 d-transition-metal carbides: a theoretical study, Phys. Rev. B 63 (2001) 134108.
[35] H.W. Hugosson, U. Jansson, B. Johansson, O. Eriksson, Phase stability diagrams of transition metal carbides, a theoretical study, Chem. Phys. Lett. 333 (2001) 444–450.
[36] L. Yang, W. Zhou, J. Jia, T. Xiong, K. Zhou, C. Feng, J. Zhou, Z. Tang, S. Chen, Nickel nanoparticles partially embedded into carbon fiber cloth via metal-mediated pitting process as flexible and efficient electrodes for hydrogen evolution reactions, Carbon 122 (2017) 710–717.
[37] W. Zhou, J. Lu, K. Zhou, L. Yang, Y. Ke, Z. Tang, S. Chen, $CoSe_2$ nanoparticles embedded defective carbon nanotubes derived from MOFs as efficient electrocatalyst for hydrogen evolution reaction, Nano Energy 28 (2016) 143–150.
[38] W. Zhou, T. Xiong, C. Shi, J. Zhou, K. Zhou, N. Zhu, L. Li, Z. Tang, S. Chen, Bioreduction of precious metals by microorganism: efficient gold@N-doped carbon electrocatalysts for the hydrogen evolution reaction, Angew. Chem. Int. Ed. 128 (2016) 8556–8560.
[39] C. Wan, B.M. Leonard, Iron-doped molybdenum carbide catalyst with high activity and stability for the hydrogen evolution reaction, Chem. Mater. 27 (2015) 4281–4288.
[40] R. Michalsky, Y.-J. Zhang, A.A. Peterson, Trends in the hydrogen evolution activity of metal carbide catalysts, ACS Catal. 4 (2014) 1274–1278.
[41] W. Cui, N. Cheng, Q. Liu, C. Ge, A.M. Asiri, X. Sun, Mo_2C nanoparticles decorated graphitic carbon sheets: biopolymer-derived solid-state synthesis and application as an efficient electrocatalyst for hydrogen generation, ACS Catal. 4 (2014) 2658–2661.
[42] D.H. Youn, S. Han, J.Y. Kim, J.Y. Kim, H. Park, S.H. Choi, J.S. Lee, Highly active and stable hydrogen evolution electrocatalysts based on molybdenum compounds on carbon nanotube-graphene hybrid support, ACS Nano 8 (2014) 5164–5173.
[43] Z. Wu, J. Wang, R. Liu, K. Xia, C. Xuan, J. Guo, W. Lei, D. Wang, Facile Preparation of carbon sphere supported molybdenum compounds (P, C and S) as hydrogen evolution electrocatalysts in acid and alkaline electrolytes, Nano Energy 32 (2017) 511–519.